

Underwater Image Enhancement With Hyper-Laplacian Reflectance Priors

Peixian Zhuang^{ID}, Jiamin Wu, Fatih Porikli^{ID}, and Chongyi Li^{ID}, Member, IEEE

Abstract—Underwater image enhancement aims at improving the visibility and eliminating color distortions of underwater images degraded by light absorption and scattering in water. Recently, retinex variational models show remarkable capacity of enhancing images by estimating reflectance and illumination in a retinex decomposition course. However, ambiguous details and unnatural color still challenge the performance of retinex variational models on underwater image enhancement. To overcome these limitations, we propose a hyper-laplacian reflectance priors inspired retinex variational model to enhance underwater images. Specifically, the hyper-laplacian reflectance priors are established with the $l_{1/2}$ -norm penalty on first-order and second-order gradients of the reflectance. Such priors exploit sparsity-promoting and complete-comprehensive reflectance that is used to enhance both salient structures and fine-scale details and recover the naturalness of authentic colors. Besides, the l_2 norm is found to be suitable for accurately estimating the illumination. As a result, we turn a complex underwater image enhancement issue into simple subproblems that separately and simultaneously estimate the reflection and the illumination that are harnessed to enhance underwater images in a retinex variational model. We mathematically analyze and solve the optimal solution of each subproblem. In the optimization course, we develop an alternating minimization algorithm that is efficient on element-wise operations and independent of additional prior knowledge of underwater conditions. Extensive experiments demonstrate the superiority of the proposed method in both subjective results and objective assessments over existing methods. The code is available at: <https://github.com/zhuangpeixian/HLRP>.

Index Terms—Underwater enhancement, retinex variational, hyper-laplacian reflectance, alternative optimization.

I. INTRODUCTION

UNDERWATER optical imaging has become an increasing research field in recent years. However, underwater

Manuscript received 5 August 2021; revised 12 June 2022; accepted 24 July 2022. Date of publication 10 August 2022; date of current version 18 August 2022. This work was supported in part by the Ministry of Science and Technology of the People's Republic of China under Grant 2020AA0108202; in part by the National Natural Science Foundation of China under Grant 62171252, Grant 61701245, and Grant 62071272; in part by the Postdoctoral Science Foundation of China under Grant 2021M701903 and Grant 2019M660644; in part by the National Key Research and Development Program of China under Grant 2020AAA0130000; and in part by the MindSpore, Compute Architecture for Neural Network (CANN), and Ascend AI Processor. The associate editor coordinating the review of this manuscript and approving it for publication was Dr. Sen-Ching Samson Cheung. (*Corresponding author: Chongyi Li.*)

Peixian Zhuang and Jiamin Wu are with the Department of Automation, Tsinghua University, Beijing 100084, China (e-mail: zhuangpeixian0624@163.com; wujiamin@tsinghua.edu.cn).

Fatih Porikli is with Qualcomm, San Diego, CA 92121 USA (e-mail: fatih.porikli@anu.edu.au).

Chongyi Li is with the School of Computer Science and Engineering, Nanyang Technological University (NTU), Singapore 639798 (e-mail: chongyi.li@ntu.edu.sg).

This article has supplementary downloadable material available at <https://doi.org/10.1109/TIP.2022.3196546>, provided by the authors.

Digital Object Identifier 10.1109/TIP.2022.3196546

image enhancement is challenging due to the complicated physical properties of underwater environments that lead to the visibility degradation and color distortion of underwater images [1]. A schematic diagram of underwater optical imaging model is illustrated in Fig. 1(a) where the light captured by the camera is mainly constituted by three components: a direct component (the light reflected from the object that has not been scattered), a forward scattering component (the light reflected from the object that has been scattered at small angles), and a backward scattering component (the light reflected not from the target object but from floating particles). An underwater image is regarded as a linear combination of these three components. The forward scattering component causes blurred image structures whereas the backward scattering veils image edges and details. Simultaneously, as shown in Fig. 1(b), different wavelengths of light are attenuated at different rates in water. Concretely, the red light first disappears since it has longest wavelength or minimum energy, while the blue and green lights show the opposite case [2]. This property results in the underwater images with bluish or greenish tone.

Many efforts have been made to promote the advancement of underwater image enhancement. Among them, retinex variational models [3]–[7] exhibit the impressive performance. Fu *et al.* [3] proposed a variational retinex enhancement model (VRE), where the luminance of color-corrected underwater image was enhanced by the l_1 norm penalty on first-order gradient of the reflectance and the l_2 norm penalized first-order gradient of the illumination. Xiong *et al.* [4] exploited Gaussian curvature priors of both reflection and illumination to construct a retinex-based variational model (GC). On the basis of above, Zhao *et al.* [5] introduced a total generalized variation prior of the illumination into the variational retinex model (TGV) [3] and combined first-order and second-order total variation to approximate piecewise smoothness and piecewise linear smoothness of the illumination. Further, a Bayesian retinex model (L1) [6] was built with imposing multi-order gradient priors on reflectance and illumination, and the l_1 norm was adopted to penalize first-order and second-order gradients of the reflectance while the l_2 norm was used to enforce spatial smoothness and spatial linear smoothness of the illumination. Besides, Cheng *et al.* [7] used a non-convex variational retinex model, with the hyper-Laplacian prior imposed on the first-order gradient of the reflectance and hybrid priors penalized on the first-order gradient of the illumination. However, different from [7], the proposed method is a retinex variational model for enhancing underwater images with multi-order gradient priors of the reflectance and illumination, where the hyper-Laplacian priors are verified to be more accurate to regularize the first-order and second-

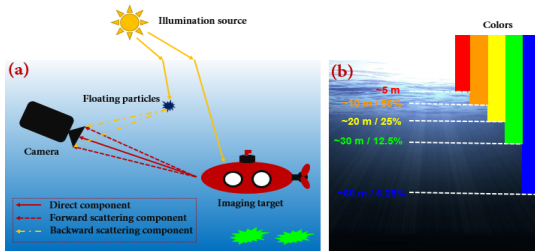


Fig. 1. Schematic diagrams of (a) underwater imaging model and (b) light attenuation at different rates in water.

order gradients of the reflectance, and the Gaussian priors are effective to regularize the first-order and second-order gradients of the illumination. Moreover, our underwater image enhancement issue is turned into three simple subproblems and its feasibility can be theoretically proved. Although the above-mentioned retinex variational models have the remarkable capacity of enhancing underwater images, two drawbacks caused by inaccurate reflectance priors are illustrated in Fig. 2. As shown in Fig. 2, 1) significant structures and fine details are ambiguous in enhanced underwater images using four retinex variational models (GC [4], VRE [3], TGV [5] and L1 [6]), and 2) color naturalness of underwater images is ineffectively preserved by these models. To overcome these limitations, we develop a novel retinex variational algorithm to enhance underwater images with hyper-laplacian reflectance priors. Our main contributions are summarized as follows:

- To the best of our knowledge, this is the first work for underwater image enhancement via the non-convex modeling on multi-order gradients of the reflectance.
- By investigating the multi-order gradient distributions of the reflectance, we found that hyper-Laplacian distributions better fit empirical distributions than Gaussian and Laplacian distributions, and the $l_{1/2}$ -norm is more accurate than the l_2 or l_1 norm for penalizing multi-order gradients of the reflectance. As a result, our method can enhance structures and fine-scale details well and effectively recovers the color of underwater images.
- We disentangle a complex underwater image enhancement issue into two simple subproblems and theoretically demonstrate its feasibility. Meanwhile, an alternating iterative optimization strategy with fast pixel-wise operations is proposed to optimize the optimal solutions.
- A large amount of experiments are conducted to demonstrate the superiority of the proposed method. Besides, two challenging applications are tested to validate the utility of our method in downstream applications.

II. RELATED WORK

Underwater image enhancement methods can be roughly organized into three main categories.

A. Model-Based Methods

The physical model-based methods first establish physical imaging models, then estimate latent model parameters with various priors or assumptions, and finally invert degradation

process to recover clear underwater scenes. With considering the physical mechanism of underwater image degradation, Drews *et al.* [8], [10] proposed an adaptation of the DCP named underwater DCP (UDCP) to estimate the underwater transmission, and made use of blue and green color channels to enable a significant improvement. Galdran *et al.* [9] presented an automatic red channel method to extract the dark channel from reversed red and blue-green channels, which recovers colors associated to short wavelengths for compensating the loss of contrast. Peng and Cosman [11] presented a depth estimation method based on image blurriness and light absorption (IBLA) to estimate more accurate background light and underwater scene depth. A generalized dark channel prior (GDCP) [12] was used to estimate underwater scene transmission according to depth-dependent color variation. The authors [13] combined DCP with wavelength-dependent compensation and image dehazing to remove the effects of haze and blur. In addition, the Sea-thru method [1] demanded the true depth map as an additional input to recover underwater color with the revised image formation model, and used spatially varying illuminant estimate to obtain the depth-dependent attenuation coefficient. In general, these model-based methods are sensitive to priors and assumptions and produce unsatisfactory results in some underwater scenes.

B. Model-Free Methods

The model-free methods adjust image pixel values to yield visually pleasing underwater images without considering physical models. Hitam *et al.* [15] built a mixture contrast limited adaptive histogram equalization to improve contrast of underwater images and reduce artifacts. Zhang *et al.* [16] extended a multi-scale retinex method for underwater image enhancement. Li *et al.* [14] made an attempt to estimate the noise map in a robust retinex model, which adopted a fidelity term for the first-order gradient of the reflectance. Under the framework [14], Ren *et al.* [18] introduced a low-rank prior into the retinex decomposition to suppress noise in the reflectance. Ancuti *et al.* [2] developed a fusion-based enhancement method to blend different filters on single underwater input, and employed a multi-scale fusion strategy by applying white balance and global contrast techniques to improve raw images. A fusion approach [17] enhanced contrast and color by blending color-compensated and white-balanced underwater images. Usually, these model-free methods are difficult to maintain better consistency of subjective and objective results. Moreover, the over-enhancement may appear in the outputs enhanced by model-free methods.

C. Data-Driven Methods

Deep learning has made significant advances on low-level vision tasks, such as image dehazing [19], denoising [20], super-resolution [21], etc. However, it is difficult to synthesize realistic underwater images for training deep networks. This is because underwater image formation models depend on lighting conditions, specific scenes, water temperature and turbidity. WaterGAN [22] was proposed to correct the color



Fig. 2. Illustration of existing retinex variational models for underwater image enhancement. Top row: raw images (Raw), the enhanced results using GC [4], VRE [3], TGV [5], L1 [6], and the proposed model (Ours). Bottom row: zoomed-in views of the red box regions of top row. Our method enhances the structure and fine-scale details well and effectively recovers the color of the underwater image.

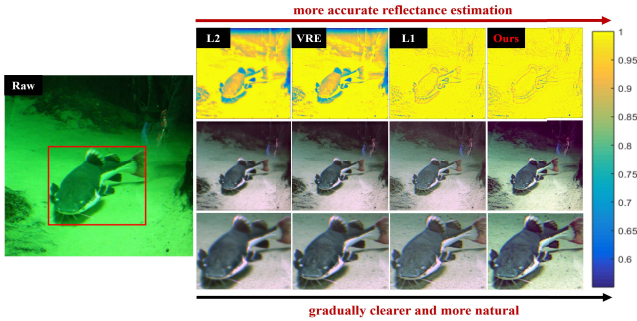


Fig. 3. Performance of different reflectance priors for enhancing underwater images. Columns 1 to 5: raw image, enhanced results using retinex variational models based on Gaussian reflectance prior $e^{-\|\nabla \mathbf{R}\|_2^2}$ (L2), Laplacian reflectance prior $e^{-\|\nabla \mathbf{R}\|_1}$ (VRE [3]), multi-order Laplacian reflectance priors $e^{-\|\nabla \mathbf{R}\|_1} \cdot e^{-\|\Delta \mathbf{R}\|_1}$ (L1 [6]), and hyper-Laplacian reflectance priors (Ours), respectively. Top row: reflectance estimations. Middle and bottom rows: enhanced images and the corresponding enlargements in the red box region of Raw. Our model adopts hyper-Laplacian reflectance priors to accurately reconstruct reflectance estimation, thus effectively overcoming the limitations of ambiguous structures and color unnaturalness.

of underwater images, which uses the generative adversarial network [23] to simulate realistic underwater images. Based on the cycle-consistent adversarial network (CycleGAN) [24], Li *et al.* [25] proposed a weakly supervised underwater color transfer model to relax the need of paired underwater images for training deep networks. An underwater generative adversarial networks [26] used the CycleGAN and simulated a degradation process to generate paired underwater images. Lately, Li *et al.* [27] synthesized paired training data based on underwater scene prior and proposed an underwater image enhancement network (UWCNN). Besides, Li *et al.* [28] constructed an Underwater Image Enhancement Benchmark (UIEB) and proposed an underwater image enhancement network (Waternet) trained on this benchmark. These data-driven methods commonly demand a large amount of underwater images for training. In addition, their robustness and generalization still lag behind conventional state-of-the-art methods.

III. MOTIVATION OF HYPER-LAPLACIAN REFLECTANCE PRIORS

The aforementioned techniques have advanced the development of underwater image enhancement, among which retinex

variational models [3]–[6] are promising alternatives to underwater image enhancement. The core of these retinex variational methods is to build a retinex variational model with different reflectance (\mathbf{R}) priors and illumination priors. Unfortunately, as previously presented in Fig. 2, significant edges and fine details of underwater images are easily ambiguous by using existing retinex variational models, along with the appearance of underwater color unnaturalness. To study the essence behind these limitations, we investigate different reflectance priors used in existing retinex variational models for enhancing underwater images as shown in Fig. 3, including Gaussian reflectance prior $e^{-\|\nabla \mathbf{R}\|_2^2}$ (L2), Laplacian reflectance prior $e^{-\|\nabla \mathbf{R}\|_1}$ (VRE [3]), multi-order Laplacian reflectance priors $e^{-\|\nabla \mathbf{R}\|_1} \cdot e^{-\|\Delta \mathbf{R}\|_1}$ (L1 [6]), and hyper-Laplacian reflectance priors (Ours), where ∇ is the first-order gradient operator and Δ is a second-order Laplacian filter.

In Fig. 3, we can see that reflectance estimations reconstructed by the L2 and VRE methods are inaccurate, which leads to ambiguous structures and color unnaturalness of enhanced underwater images. Although the L1 method adds second-order gradient prior of the reflectance to compensate for accurate estimation of the reflectance, unsatisfactory results of both structural restoration and color naturalness are still existing in the enhanced image and corresponding enlargement. Tracing back to the reason, these limitations of retinex variational models are caused by inaccurate reflectance priors.

To achieve more accurate reflectance priors, we develop hyper-Laplacian reflectance priors that consist of first-order gradient reflectance prior $e^{-\|\nabla \mathbf{R}\|_{1/2}}$ and second-order gradient reflectance prior $e^{-\|\Delta \mathbf{R}\|_{1/2}}$. To be specific, we collected 100 high quality underwater images displayed in Fig. 4(a) where various underwater scenes contain different types of underwater objects, background color, and luminance. Following previous works [3], [6], we converted each underwater image from RGB color space to HSV color space that is more robust to the illumination variations [29]. Based on the retinex theory [30], the value channel in the HSV color space is decomposed into the reflectance component \mathbf{R} and the illumination component \mathbf{I} . In Fig. 4(c-e), we plot the fitting curves to empirical first-order ($\nabla \mathbf{R}$) and second-order ($\Delta \mathbf{R}$) gradient distributions of the reflectance in the logarithm domain. The empirical first-order and second-order gradient data (black star-dot) are generated by averaging on the reflectances of the 100 high quality underwater images, along with fitting Gaussian ($e^{-\|\nabla \mathbf{R}\|_2^2}$ and $e^{-\|\Delta \mathbf{R}\|_2^2}$, blue solid-line), Laplacian ($e^{-\|\nabla \mathbf{R}\|_1}$ and $e^{-\|\Delta \mathbf{R}\|_1}$, green solid-line), and

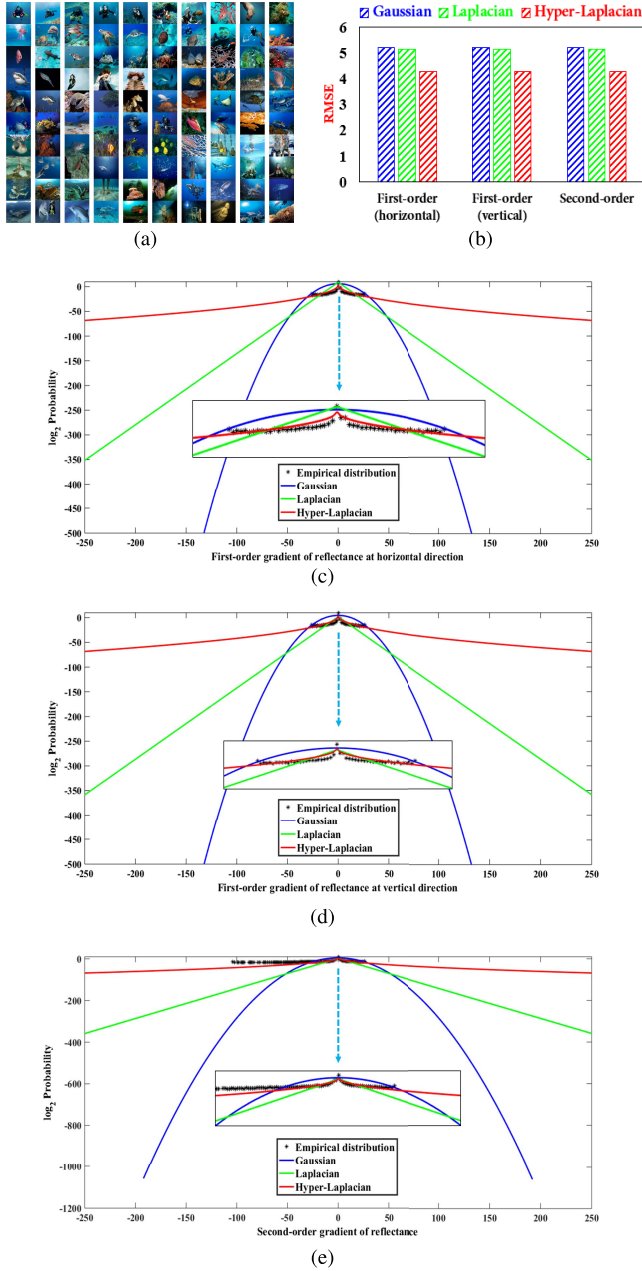


Fig. 4. Statistic of hyper-Laplacian reflectance priors. (a) A snapshot of 100 high quality underwater images. (c-e) Fitting curves to multi-order gradient distributions of reflectance in log domain. The empirical multi-order gradient data (black star-dot) are generated by averaging on the reflectances of the 100 high quality underwater images, along with fitting Gaussian (l_2 norm, blue solid-line), Laplacian (l_1 norm, green solid-line), and hyper-Laplacian ($l_{1/2}$ norm, red solid-line) distributions. As shown, the hyper-Laplacian distributions better fit the empirical distributions than the Gaussian and Laplacian distributions. (b) The root mean squared errors (RMSE) correspond to (c-e). The hyper-Laplacian distributions yield smaller RMSE than the Gaussian and Laplacian distributions in multi-order gradient domains.

hyper-Laplacian ($e^{-\|\nabla \mathbf{R}\|_{1/2}}$ and $e^{-\|\Delta \mathbf{R}\|_{1/2}}$, red solid-line) distributions. Meanwhile, Fig. 4(b) reports the root mean squared errors (RMSE) corresponding to Fig. 4(c-e). By studying the above results, we draw that the empirical distributions of multi-order gradient data are highly peaked at zero and can be well approximated by the hyper-Laplacian distributions, while the Gaussian and Laplacian distributions yield larger

fitting errors. Thus, the hyper-Laplacian distributions better fit the empirical distributions than the Gaussian and Laplacian distributions. Consequently, this finding motivates us to model first-order and second-order gradients of the reflectance with hyper-Laplacian priors, named hyper-Laplacian reflectance priors $e^{-\|\nabla \mathbf{R}\|_{1/2}} \cdot e^{-\|\Delta \mathbf{R}\|_{1/2}}$. Correspondingly in the form of optimization modeling, the $l_{1/2}$ norm is more accurate than both the l_2 norm and the l_1 norm for the reflectance penalty.

Further, we couple the proposed hyper-laplacian reflectance priors with the same retinex variational framework as other methods for enhancing underwater images. Fig. 3 suggests that the proposed hyper-Laplacian reflectance priors can reconstruct more accurate reflectance estimation, and are effective in overcoming the limitations of ambiguous structures and color unnaturalness. Therefore, our method yields preferable results when compared with other retinex variational models that employ the Gaussian and Laplacian reflectance priors. The consistency results are also presented in Fig. 2, where hyper-laplacian reflectance priors are capable of enhancing edges and details and recovering colors.

We dissect multi-order gradient priors of reflectance and illumination in the HSV color space. The results corresponding to two examples are presented in Fig. 5, where we observe that there are abundant image edges and details in first-order and second-order gradients of the reflectance. An intriguing finding is that the reflectance contains significant edges and fine-scale details, and the histogram distributions of its multi-order gradients are more sparse than those of the illumination, which is consistent with the above-mentioned hyper-Laplacian priors. On the contrary, the illumination is found to present relative smoother than the reflectance. This finding supports that the l_2 norm is appropriate and efficient to model first-order ($\nabla \mathbf{I}$) and second-order ($\Delta \mathbf{I}$) gradients of the illumination with Gaussian smoothing priors ($e^{-\|\nabla \mathbf{I}\|_2^2}$ and $e^{-\|\Delta \mathbf{I}\|_2^2}$).

IV. OUR METHOD

The overview of the proposed method is shown in Fig. 6. First, a simple yet effective color correction based on statistical method [3] is adopted to restore both color and naturalness of a degraded underwater image \mathbf{O} . Then, following works [3], [31], [32] that avoid potential color artifacts and reduce computational complexity, the color-corrected underwater image \mathbf{U} is converted from RGB color space to HSV color space that is more robust to illumination variations. Thus the retinex theory [30] can handle the illumination that adaptively varies brightness and color. Next, we adopt the retinex model to deal with the value channel. The value channel \mathbf{V} in the HSV color space is first decomposed into the reflectance layer \mathbf{R} and the illumination layer \mathbf{I} . The proposed retinex variational model with hyper-Laplacian reflectance priors is performed to enhance \mathbf{R} and \mathbf{I} simultaneously. After that, a Gamma correction scheme [31], [32] method is used to adjust the enhanced illumination \mathbf{I}_e and thus the enhanced value channel \mathbf{V}_e is generated by a product of the enhanced reflectance and the adjusted illumination \mathbf{I}_e . At last, the final enhanced image is yielded by converting the enhanced HSV image to

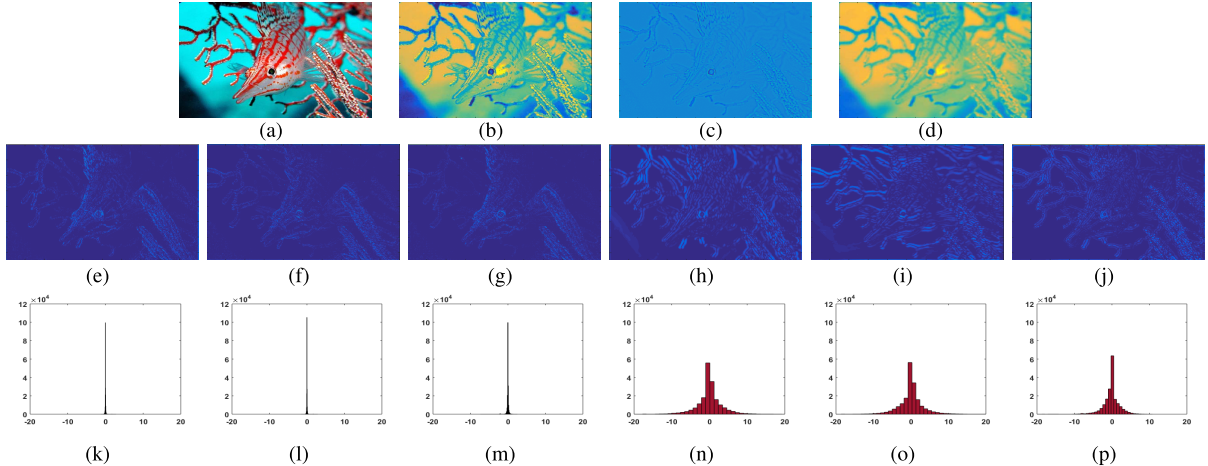


Fig. 5. Multi-order gradient priors of reflectance and illumination in HSV color space. (a) high-quality underwater image. (b) the value channel. (c) the reflectance. (d) the illumination. (e)-(f) and (h)-(i): first-order gradient in horizontal and vertical directions of (c) and (d), respectively. (g) and (j): second-order gradient of (c) and (d), respectively. (k)-(p): corresponding histograms of (e)-(j), respectively. There are abundant structures in first-order and second-order gradients of the reflectance. The reflectance contains significant edges and fine-scale details, and its multi-order gradients have more sparse histogram distributions than those of the illumination. The illumination presents relative smoother than the reflectance.

RGB color space. We detail model construction and numerical optimization of the proposed method as follows.

A. Model Construction

The color corrected \mathbf{U} is first converted from RGB color space to HSV color space that is more stabilized to illumination variations. Based on the retinex theory [30], \mathbf{V} is decomposed into the reflectance \mathbf{R} and the illumination \mathbf{I} . After that, the proposed retinex variational model with hyper-Laplacian reflectance priors is performed to enhance \mathbf{R} and \mathbf{I} . By Bayes theorem, the retinex probabilistic model for enhancing \mathbf{R} and \mathbf{I} is established as a posterior distribution:

$$p(\mathbf{R}, \mathbf{I}|\mathbf{V}) \propto p(\mathbf{V}|\mathbf{R}, \mathbf{I})p(\mathbf{R})p(\mathbf{I}), \quad (1)$$

where $p(\mathbf{R}, \mathbf{I}|\mathbf{V})$ is the posterior distribution, $p(\mathbf{V}|\mathbf{R}, \mathbf{I})$ is the likelihood, $p(\mathbf{R})$ and $p(\mathbf{I})$ denote the priors on the reflectance and the illumination, respectively. As follows, we define these terms and then describe our numerical optimization.

1) *Likelihood $p(\mathbf{V}|\mathbf{R}, \mathbf{I})$* : The retinex decomposition model is expressed as $\mathbf{V} = \mathbf{R} \odot \mathbf{I}$, the value channel \mathbf{V} is ideally seen as a product of the reflectance \mathbf{R} and the illumination \mathbf{I} , where \odot denotes the element-wise multiplication. The estimated error $\mathbf{e} = \mathbf{V} - \mathbf{R} \odot \mathbf{I}$ is generally modeled as a set of independent and identically distributed noise random variables with a Gaussian distribution of zero mean and variance σ^2 . The likelihood $p(\mathbf{V}|\mathbf{R}, \mathbf{I})$ is defined as

$$p(\mathbf{V}|\mathbf{R}, \mathbf{I}) = \mathcal{N}(\mathbf{e}|0, \sigma^2 \mathbf{I}), \quad (2)$$

where \mathbf{I} represents the identity matrix.

2) *Hyper-Laplacian Reflectance Priors $p(\mathbf{R})$* : Fig. 3 has shown that multi-order gradient reflectance priors ($e^{-\|\nabla \mathbf{R}\|_1} \cdot e^{-\|\Delta \mathbf{R}\|_1}$, L1 [6]) outperform single-order gradient reflectance prior ($e^{-\|\nabla \mathbf{R}\|_1}$, VRE [3]) in terms of reflectance estimation accuracy and underwater structure enhancement. Then as seen from Fig. 5(e)-(g), there are abundant underwater image structures, containing significant edges and fine-scale details,

in first-order and second-order gradients of the reflectance. These results suggest that multi-order gradient priors are suitable for underwater structure enhancement. For capturing complete structures and fine-scale details from underwater images, multi-order gradient priors are adopted to design $p(\mathbf{R})$. We found that the histograms of multi-order gradients of the reflectance (e.g., Fig. 5(k)-(m)) appear more sparse than those of the illumination (e.g., Fig. 5(n)-(p)). Additionally, the results of Fig. 4 indicate that the empirical distributions of multi-order gradient of the reflectance are better approximated by the hyper-Laplacian distributions, while the Gaussian and Laplacian distributions yield larger fitting errors. Eventually, these findings inspire us to model first-order and second-order gradients of the reflectance with the hyper-Laplacian priors, and the $l_{1/2}$ norm is more accurate than the l_2 and l_1 norms for the reflectance. Therefore, first-order ($\nabla \mathbf{R}$) and second-order ($\Delta \mathbf{R}$) gradient distributions of the reflectance can be defined as hyper-Laplacian distributions with location zero and scales s_1, s_2 ,

$$p(\nabla \mathbf{R}) = \mathcal{H}\mathcal{L}(\nabla \mathbf{R}|0, s_1 \mathbf{I}), \quad (3)$$

$$p(\Delta \mathbf{R}) = \mathcal{H}\mathcal{L}(\Delta \mathbf{R}|0, s_2 \mathbf{I}), \quad (4)$$

where $\mathcal{H}\mathcal{L}(x|0, s) = e^{-\frac{|x|^{\frac{1}{2}}}{s}}$ is an element-wise representation form of hyper-Laplacian distribution with the $l_{1/2}$ norm, and the second-order Laplacian filter $\Delta = [0, 1, 0; 1, -4, 1; 0, 1, 0]$.

Hyper-Laplacian reflectance priors $p(\mathbf{R})$ are defined as

$$p(\mathbf{R}) = p(\nabla \mathbf{R})p(\Delta \mathbf{R}), \quad (5)$$

3) *Gaussian-Smoothing Illumination Priors $p(\mathbf{I})$* : To acquire complementary and complete structures from underwater images, multi-order gradient priors are imposed to enforce spatial smoothness and spatial linear smoothness of the illumination. By observing Fig. 5(h)-(j), we found that substantial smooth structures are in first-order and second-order gradients of the illumination, complementary to those of

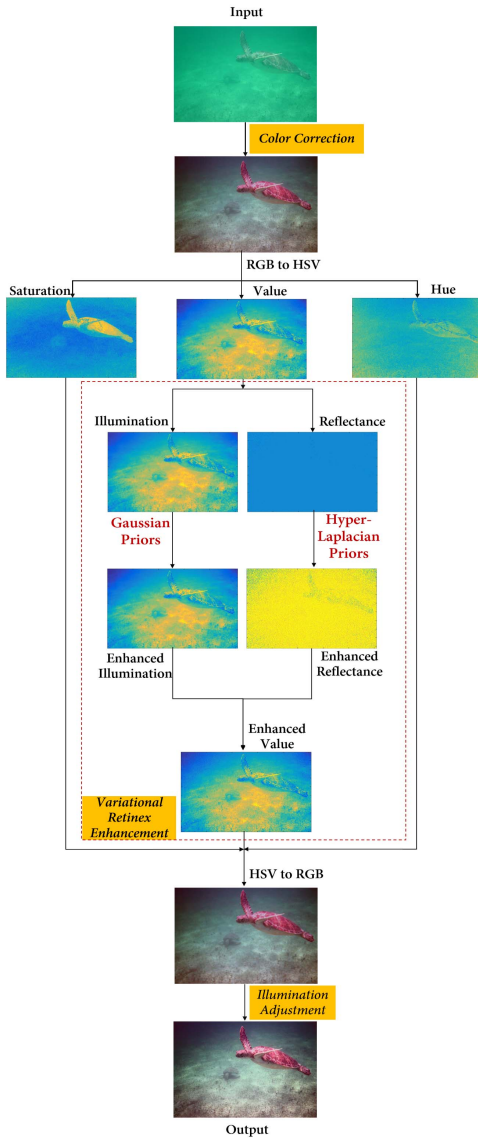


Fig. 6. Flowchart of the proposed method.

the reflectance. As seen in Figs. 5(h)-(j) and (n)-(p), we found that the illumination has complementary structures and its multi-order histograms are shown to be relative smoother than those of the reflectance. This finding motivates that the Gaussian distributions of zero mean and variances σ_3^2 , σ_4^2 are adopted to model first-order ($\nabla \mathbf{I}$) and second-order ($\Delta \mathbf{I}$) gradient priors of the illumination,

$$p(\nabla \mathbf{I}) = \mathcal{N}(\nabla \mathbf{I} | 0, \sigma_3^2 \mathbf{1}), \quad (6)$$

$$p(\Delta \mathbf{I}) = \mathcal{N}(\Delta \mathbf{I} | 0, \sigma_4^2 \mathbf{1}), \quad (7)$$

Gaussian smoothing illumination priors $p(\mathbf{I})$ are expressed as

$$p(\mathbf{I}) = p(\nabla \mathbf{I}) p(\Delta \mathbf{I}), \quad (8)$$

In addition, the constrain $\mathbf{V} \leq \mathbf{I}$ guarantees the prior that \mathbf{R} is in the range of [0,1].

4) Final Objective $E(\mathbf{R}, \mathbf{I})$: The maximum a posteriori (MAP) problem Eq. (1) is transformed to an energy

minimization problem that jointly estimates the reflectance and the illumination, i.e., $E(\mathbf{R}, \mathbf{I}) = -\log(p(\mathbf{R}, \mathbf{I} | \mathbf{V}))$. We take the likelihood Eq. (2), hyper-Laplacian reflectance priors Eq. (5), illumination priors Eq. (8) and illumination constrain into Eq. (1), and the final objective function $E(\mathbf{R}, \mathbf{I})$ is established:

$$\begin{aligned} E(\mathbf{R}, \mathbf{I}) = & \|\mathbf{R} \odot \mathbf{I} - \mathbf{V}\|_2^2 + \lambda_1 \|\nabla \mathbf{R}\|_{1/2} + \lambda_2 \|\Delta \mathbf{R}\|_{1/2} \\ & + \zeta_1 \|\nabla \mathbf{I}\|_2^2 + \zeta_2 \|\Delta \mathbf{I}\|_2^2 \quad \text{s.t. } \mathbf{V} \leq \mathbf{I}, \end{aligned} \quad (9)$$

where these scale parameters ($\lambda_i = \sigma^2/s_i$ when $i = 1, 2$, and $\zeta_i = \sigma^2/\sigma_i^2$ when $i = 3, 4$) are positive to balance above terms. The role of each term in Eq. (9) is explained as follows. 1) $\|\mathbf{R} \odot \mathbf{I} - \mathbf{V}\|_2^2$ is the data fidelity that imposes the l_2 norm to enforce the consistency of $\mathbf{R} \odot \mathbf{I}$ to \mathbf{V} . 2) $\|\nabla \mathbf{R}\|_{1/2}$ and $\|\Delta \mathbf{R}\|_{1/2}$ are the reflectance penalty that adopts the accurate $l_{1/2}$ norm to enforce the sparsity of first-order and second-order gradients of the reflectance, corresponding to hyper-Laplacian reflectance priors. 3) $\|\nabla \mathbf{I}\|_2^2$ and $\|\Delta \mathbf{I}\|_2^2$ are the illumination penalty that applies the appropriate l_2 norm to enforce the sparsity of first-order and second-order gradients of the illumination, with respect to Gaussian-smoothing illumination priors. 4) $\mathbf{V} \leq \mathbf{I}$ denotes the illumination constraint to ensure $\mathbf{R} \in [0,1]$.

B. Numerical Optimization

To address the minimization problem Eq. (9) where there are two unknown variables \mathbf{R} and \mathbf{I} , we develop an efficient alternating iteration optimization strategy to find a local optimal solution to the non-convex objective function via the alternating direction method of multipliers (ADMM) [33] with iterative half thresholding [34], [35] and fast Fourier transform (FFT) [36]. It is intractable to directly optimize Eq. (9) due to two non-convex $l_{1/2}$ norms, therefore, two auxiliary variables \mathbf{d} , \mathbf{h} and two errors \mathbf{m} , \mathbf{n} are introduced to reformulate Eq. (9) into the following form:

$$\begin{aligned} E(\mathbf{R}, \mathbf{I}) = & \|\mathbf{R} \odot \mathbf{I} - \mathbf{V}\|_2^2 + \lambda_1 \{\eta_1 \|\mathbf{d}\|_{1/2} + \|\nabla \mathbf{R} - \mathbf{d} + \mathbf{m}\|_2^2\} \\ & + \lambda_2 \{\eta_2 \|\mathbf{h}\|_{1/2} + \|\Delta \mathbf{R} - \mathbf{h} + \mathbf{n}\|_2^2\} + \zeta_1 \|\nabla \mathbf{I}\|_2^2 \\ & + \zeta_2 \|\Delta \mathbf{I}\|_2^2 \quad \text{s.t. } \mathbf{V} \leq \mathbf{I}, \end{aligned} \quad (10)$$

where η_1 and η_2 are positive parameters to weigh above terms.

Then, the complex problem Eq. (10) is decomposed into three simple subproblems which can be individually optimized and iteratively cycled through. Their forms at the k th iteration are written:

$$\begin{aligned} (P1) \quad \mathbf{d}^k = & \arg \min_{\mathbf{d}} \|\nabla \mathbf{R}^{k-1} - \mathbf{d} + \mathbf{m}^{k-1}\|_2^2 + \eta_1 \|\mathbf{d}\|_{1/2}, \\ \mathbf{h}^k = & \arg \min_{\mathbf{h}} \|\Delta \mathbf{R}^{k-1} - \mathbf{h} + \mathbf{n}^{k-1}\|_2^2 + \eta_2 \|\mathbf{h}\|_{1/2}, \end{aligned} \quad (11)$$

$$\begin{aligned} (P2) \quad \mathbf{R}^k = & \arg \min_{\mathbf{R}} \left\| \frac{\mathbf{V}}{\mathbf{I}^{k-1}} \right\|_2^2 + \lambda_1 \|\nabla \mathbf{R} - \mathbf{d}^k + \mathbf{m}^{k-1}\|_2^2 \\ & + \lambda_2 \|\Delta \mathbf{R} - \mathbf{h}^k + \mathbf{n}^{k-1}\|_2^2, \\ \mathbf{m}^k = & \mathbf{m}^{k-1} + \nabla \mathbf{R}^k - \mathbf{d}^k, \\ \mathbf{n}^k = & \mathbf{n}^{k-1} + \Delta \mathbf{R}^k - \mathbf{h}^k, \end{aligned} \quad (12)$$

$$(P3) \quad \mathbf{I}^k = \arg \min_{\mathbf{I}} \left\| \frac{\mathbf{V}}{\mathbf{R}^k} \right\|_2^2 + \zeta_1 \|\nabla \mathbf{I}\|_2^2 + \zeta_2 \|\Delta \mathbf{I}\|_2^2, \quad (13)$$

Note that $\|\mathbf{R} \cdot \mathbf{I}^{k-1} - \mathbf{V}\|_2^2$ and $\|\mathbf{I} \cdot \mathbf{R}^k - \mathbf{V}\|_2^2$ are respectively transformed into $\|\mathbf{R} - \frac{\mathbf{V}}{\mathbf{I}^{k-1}}\|_2^2$ and $\|\mathbf{I} - \frac{\mathbf{V}}{\mathbf{R}^k}\|_2^2$ for convenience. These subproblems have closed-form solutions and their updates are detailed below.

Update (P1): Iterative Half Thresholding. First initialize $\mathbf{R}^0 = 0$, $\mathbf{m}^0 = 0$, $\mathbf{n}^0 = 0$. Then an iterative half thresholding algorithm [34], [35] is adopted to update the auxiliary variables \mathbf{d}^k and \mathbf{h}^k at the k th iteration:

$$\begin{aligned}\mathbf{d}_h^k &= \mathbf{H}_{\eta_1\mu,\frac{1}{2}}(\mathbf{d}_h^{k-1} - \mu(\mathbf{d}_h^{k-1} - \nabla_h \mathbf{R}^{k-1} - \mathbf{m}_h^{k-1})), \\ \mathbf{d}_v^k &= \mathbf{H}_{\eta_1\mu,\frac{1}{2}}(\mathbf{d}_v^{k-1} - \mu(\mathbf{d}_v^{k-1} - \nabla_v \mathbf{R}^{k-1} - \mathbf{m}_v^{k-1})), \\ \mathbf{h}^k &= \mathbf{H}_{\eta_2\mu,\frac{1}{2}}(\mathbf{h}^{k-1} - \mu(\mathbf{h}^{k-1} - \Delta \mathbf{R}^{k-1} - \mathbf{n}^{k-1})),\end{aligned}\quad (14)$$

where $\mathbf{H}_{\eta_1\mu,\frac{1}{2}}(\cdot)$ and $\mathbf{H}_{\eta_2\mu,\frac{1}{2}}(\cdot)$ denote the half thresholding operators concretely defined in [34] and [35]. $\mu > 0$ is a step size parameter which is generally set to the reciprocal of the total number of image pixels. $\nabla_h = [-1, 1]$ and $\nabla_v = [-1; 1]$ denote first-order derivative operator at horizontal and vertical directions, respectively.

Update (P2): Reflectance Reconstruction. Like center/surround retinex methods [37], [38], a Gaussian lowpass filtering of \mathbf{V} is used to be an initialization of \mathbf{I}^0 . Since (P2) is a least square problem that includes three convex functions, the first-order derivative of Eq. (12) is set to 0, and the fast Fourier transformation (FFT) [36] is used to accelerate the solution process. The closed-form solution \mathbf{R}^k is updated:

$$\mathbf{R}^k = \mathcal{F}^{-1}\left\{\frac{\mathcal{F}(\mathbf{V}/\mathbf{I}^{k-1}) + \lambda_1 \Psi_1 + \lambda_2 \Psi_2}{\mathcal{F}(\mathbf{1}) + \lambda_1 \Phi_1 + \lambda_2 \Phi_2}\right\}, \quad (15)$$

where \mathcal{F} denotes the FFT operator, \mathcal{F}^* and \mathcal{F}^{-1} are conjugate transpose and inverse operators of \mathcal{F} , respectively. $\Psi_1 = \mathcal{F}^*(\nabla_h) \odot \mathcal{F}(\mathbf{d}_h^k - \mathbf{m}_h^{k-1}) + \mathcal{F}^*(\nabla_v) \odot \mathcal{F}(\mathbf{d}_v^k - \mathbf{m}_v^{k-1})$, $\Psi_2 = \mathcal{F}^*(\Delta) \odot \mathcal{F}(\mathbf{h}^k - \mathbf{n}^{k-1})$, $\Phi_1 = \mathcal{F}^*(\nabla_h) \odot \mathcal{F}(\nabla_h) + \mathcal{F}^*(\nabla_v) \odot \mathcal{F}(\nabla_v)$, and $\Phi_2 = \mathcal{F}^*(\Delta) \odot \mathcal{F}(\Delta)$. The first-order and second-order derivative operators can be diagonalized by using the FFT for avoiding large-scale matrix inversion, and all operations of above calculations are performed component-wise. Following ADMM, \mathbf{m}^k and \mathbf{n}^k are updated by

$$\begin{aligned}\mathbf{m}_h^k &= \mathbf{m}_h^{k-1} + \nabla_h \mathbf{R}^k - \mathbf{d}_h^k, \\ \mathbf{m}_v^k &= \mathbf{m}_v^{k-1} + \nabla_v \mathbf{R}^k - \mathbf{d}_v^k, \\ \mathbf{n}^k &= \mathbf{n}^{k-1} + \Delta \mathbf{R}^k - \mathbf{h}^k,\end{aligned}\quad (16)$$

Update (P3): Illumination Reconstruction. Similar to above reflectance reconstruction, (P3) is a least square problem including three convex functions, and the first-order derivative of Eq. (13) is set to 0, then the FFT is adopted to speed up the solving process. Finally, the closed-form solution of the illumination \mathbf{I}^k is updated by

$$\mathbf{I}^k = \mathcal{F}^{-1}\left\{\frac{\mathcal{F}(\mathbf{V}/\mathbf{R}^k)}{\mathcal{F}(\mathbf{1}) + \zeta_1 \Phi_1 + \zeta_2 \Phi_2}\right\}, \quad (17)$$

All operations of above calculations are performed component-wise. With respect to the illumination constraint $\mathbf{V} \leq \mathbf{I}$ in Eq. (10), following the previous work [3], the updated illumination is corrected through $\mathbf{I}^k = \max(\mathbf{I}^k, \mathbf{V})$.

Element-wise operations of FFT and half thresholding are fast implemented at few iterations. \mathbf{I} and \mathbf{R} are efficiently and

jointly estimated. The main steps of the proposed algorithm are sketched in **Algorithm 1**. What is more, the convergence of the proposed algorithm is theoretically proved in the supplementary material¹.

Algorithm 1 Outline of Optimizing E in Eq. (10)

Input: input value channel \mathbf{V} , regularization parameters $\{\lambda_i\}_{i=1}^2$ and $\{\zeta_i\}_{i=1}^2$, thresholding parameters $\{\eta_i\}_{i=1}^2$, and maximum iteration T .

Initialization: $\mathbf{I}^0 \leftarrow$ Gaussian filtering of \mathbf{V} , $\mathbf{R}^0 = 0$, $\mathbf{m}^0 = 0$, $\mathbf{n}^0 = 0$, and $k = 1$.

Iteration on $k = 1, \dots, T$:

update \mathbf{d}^k and \mathbf{h}^k via Eq. (14).

update \mathbf{R}^k via Eq. (15).

update \mathbf{m}^k and \mathbf{n}^k via Eq. (16).

update \mathbf{I}^k via Eq. (17).

Stopping criteria: terminate iteration if $k = T$, otherwise, continue iteration and $k \leftarrow k + 1$.

Output: reconstructed reflectance \mathbf{R} and illumination \mathbf{I} .

V. EXPERIMENTAL RESULTS AND DISCUSSION

To demonstrate the superior performance of the proposed method, qualitative evaluation, quantitative assessment, ablation study, and application test are conducted respectively. Due to the limited space, more experimental results can be found in the supplementary material¹.

Test Data. We first conduct comparisons on a large number of underwater images that contain various scenes and diverse degradations, where 300 underwater images are collected from [2], [3], [9], [13], [28], [39], [40]. We then perform comparative experiments on 60 challenging underwater images from the Underwater Image Enhancement Benchmark Dataset (UIEBD) [28], which includes mist and under-exposure underwater images in deep sea with non-uniform illumination, and turbid and yellowish underwater images due to strongly attenuated blue channels. Besides, we implement an experiment of enhancing a challenging underwater video that involves 1500 frames with five types of degenerate colors.

Parameter Settings. In following experiments, the regularization parameters λ_1 , λ_2 , ζ_1 and ζ_2 are set to $1e-4$, $1e-3$, $1e-5$ and $1e-3$, respectively. Half thresholding parameters η_1 and η_2 are set to $1e-3$. The number of maximum iteration T is set to 5 for a trade-off between algorithm convergence and computation efficiency. The proposed method is insensitive to the parameter setting, and this reason lies on that the parameters λ_1 and λ_2 control the regularization degree of multi-order reflectance gradients, the parameters ζ_1 and ζ_2 control the regularization degree of multi-order illumination gradients, and the parameters η_1 and η_2 change the thresholding step in the iterative half thresholding operation. These parameters are independent on input image type. The empirical settings of all parameters in our method are universal for different test data.

¹<https://github.com/zhuangpeixian/HLRP>

Compared Methods. We compare our method against eight methods, including two retinex variational methods (VRE [3] and L1 [6]), one model-free method (CBF [17]), three model-based methods (UDCP [10], IBLA [11], GDCP [12]), two data-driven methods (UWCNN [27] and Waternet [28]). We use the released codes of VRE [3], UDCP [10], UWCNN [27], Waternet [28], and L1 [6] to yield their results. We use the code of CBF [17] re-implemented by other researchers to produce results. The execution codes of IBLA [11] and GDCP [12] are provided by the authors. For UWCNN [27], we adopt the UWCNN-typeI model because of its more robust performance. In order to make a fair comparison, we refer to corresponding literatures and set their parameters according to default settings suggested by the authors.

Evaluation Metrics. For the 300 underwater images without the corresponding ground truth images, we employ the four non-reference evaluation metrics UIQM [41], UCIQE [42], PCQI [43], and Entropy [39] to measure the performance of different methods. UIQM is a linear composition of UISM (Underwater Image Sharpness Measure), UIConM (Underwater Image Contrast Measure), and UICM. A higher UIQM indicates a better tradeoff among sharpness, contrast, and colorfulness. UCIQE is a linear combination of chroma, saturation, and contrast (Con_l), which quantifies nonuniform color cast, blurring, and low-contrast. A higher UCIQE suggests a better tradeoff among chroma, saturation, and contrast. PCQI assesses perceptual distortions between enhanced and raw images from mean intensity, signal strength and structure. A larger PCQI means better contrast quality. Entropy represents average information of an image. A higher Entropy indicates more information contained in the image. Further, we use the four non-reference metrics UISM, UIConM, Con_l , and NVE (Number of restored Visible Edges in blind contrast enhancement assessment [44]) to assess structure and contrast enhancement performance of all methods, and higher values of these indicators suggest better results of structure and contrast enhancement. To evaluate color correction accuracy of all methods, we use two full-reference metrics PSNR and RMSE to compute the color dissimilarity between the ground-truth ColorChecker and their results, and one non-reference metric LOE (lightness order error [49]) to measure the color distortion between the ColorChecker in the raw image and the results in the enhanced images. A higher PSNR or a lower RMSE means that the result is closer to the ground-truth color. A lower LOE denotes that the result is less degraded from color distortion.

A. Qualitative Evaluation

We first conduct visual comparisons of different methods on the 300 underwater images. Visual results of underwater images with different color degradations are shown in Figs. 7-9. As shown, our method can solve the limitations of ambiguous structure and color unnaturalness that appear in both VRE and L1 with Laplacian reflectance priors. In comparison, our method outperforms other methods in terms of structures and details enhancement, color and naturalness rehabilitation, contrast promotion and artifacts suppression.

TABLE I

QUANTITATIVE MEASUREMENTS OF DIFFERENT METHODS AVERAGED ON THE 300 UNDERWATER IMAGES. THE BEST RESULT IS IN RED UNDER EACH CASE

Methods	UIQM \uparrow	UCIQE \uparrow	PCQI \uparrow	Entropy \uparrow
Raw	2.195	0.511	1.000	6.939
VRE [3]	4.028	0.597	1.008	7.627
UDCP [10]	3.735	0.597	0.946	7.109
IBLA [11]	2.842	0.595	1.091	7.348
CBF [17]	3.914	0.589	1.107	7.423
GDCP [12]	3.476	0.587	1.095	7.343
UWCNN [27]	3.725	0.493	0.809	6.592
Waternet [28]	3.748	0.566	0.964	7.166
L1 [6]	4.089	0.582	1.125	7.718
Ours	4.133	0.647	1.203	7.884

UDCP aggravates color casts and poorly performs in contrast improvement. IBLA has positive impacts on color correction and contrast improvement, but an over-enhanced result is seen in the first comparison image of Fig. 7. Although underwater image structures are improved by CBF, white-balanced results are shown in Figs. 7 and 8. GDCP restores underwater image colors and structures, but over-brightness results present in the enhanced images. UWCNN has poor results of color recovery and structure improvement when training on special types of synthetic underwater images. Waternet turns raw images into good results of color correction and contrast improvement, however, color naturalness and detail enhancement are suboptimal in Figs. 7 and 9. By contrast, our method can robustly recover colors and naturalness and significantly enhance structures and contrast when enhancing various types of underwater images, which suggests that our hyper-Laplacian reflectance priors are effective in different underwater scenes.

Then, we demonstrate the advantage of the proposed method on the 60 challenging underwater images. Fig. 10 shows the enhanced results using different methods on four typical underwater images. UDCP and UWCNN fail to remove undesirable yellow layers and produce color distortions in the enhanced images. IBLA and GDCP acquire better contrast but cannot completely eliminate yellow interferences, and reddish deviations appear in their results. CBF and Waternet clean yellowish layers and enhance structures, but introduce artificial purple colors in the third comparison image. Compared with both VRE and L1, our method is superior to enhancing structure and contrast and restoring authentic color and naturality. Clearer details and more natural colors are yielded by the proposed method, which demonstrates the robustness of our method in challenging underwater scenes. Besides, we perform an experiment of enhancing a challenging underwater video to show the scalability of our model. The enhanced video by our method is available in the supplementary material, and partial results are exhibited in Fig. 11. Our method can clean color casts, recover color naturalness, and boost structures and contrasts. Additionally, our results of different frames are consistent and impressive in various underwater scenes.

We further test the ColorChecker 24 X-Rite Chart image [39] to exhibit color correction accuracy of our method. As shown in Fig. 12, our method is superior to both VRE

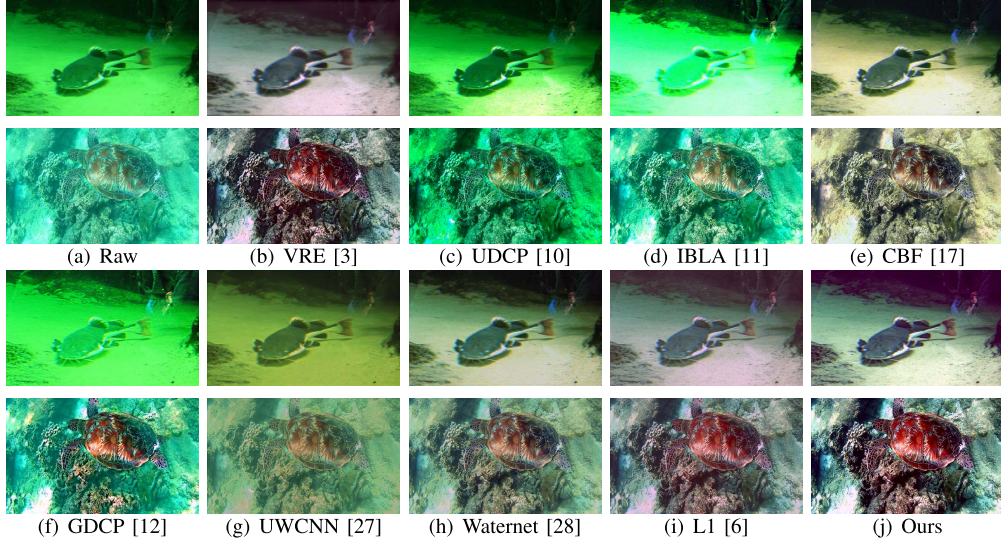


Fig. 7. Visual comparison of different methods on greenish underwater images.

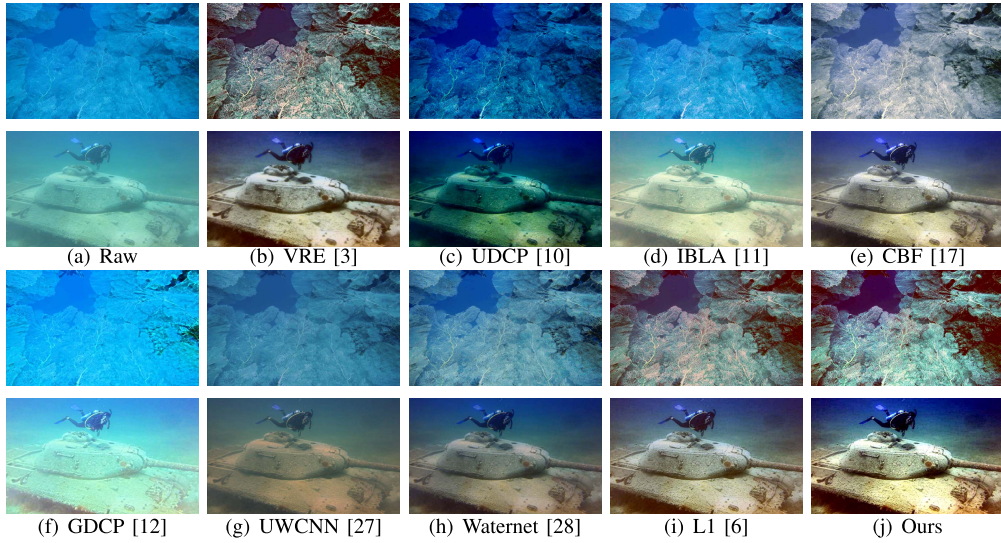


Fig. 8. Visual comparison of different methods on bluish underwater images.

and L1 in terms of color detail enhancement and color naturalness restoration. UDCP and IBLA recover most colors but cannot remove color casts in the fourth row and second or third column. CBF has impressive color restoration, but tends to generate over-whitened results. UWCNN fails to recover authentic color and presents entire darkness. Waternet restores color tone but cannot yield more color details. In comparison, our method is capable of removing color casts and unveiling more color details. This test results suggest the superiority of our method in rehabilitating genuine underwater colors.

B. Quantitative Assessment

We quantify the performance of different methods in terms of UIQM, UCIQE, PCQI, and Entropy on the 300 underwater images. Table I reports the average values of four metrics. As presented, our method outperforms both VRE and L1 in terms of UIQM, UCIQE, PCQI and Entropy, which demonstrates that our hyper-Laplacian reflectance priors are more

superior to overcoming the limitations of ambiguous structure and color unnaturalness. Compared with the rest methods, our method achieves a higher UIQM value, which suggests better performance of our method in colorfulness restoration and structure enhancement. Our method yields the best Entropy and recovers more information of underwater images. The best UCIQE by our method is with respect to a promising ability of removing non-uniform color casts and blurring and promoting local details and global contrast. Moreover, the best PCQI by our method is superior to other methods, which indicates that our method is more effective in narrowing perceptual distortions between enhanced and raw underwater images. In comparison, our method yields better metric values, which corresponds to remarkable structure and contrast improvement and preferable color and naturalness restoration.

Further, we compare our method with the eight methods on raw underwater images with four typical color degradations. In Table II, five metrics UISM, UIConM, Con_l , NVE and

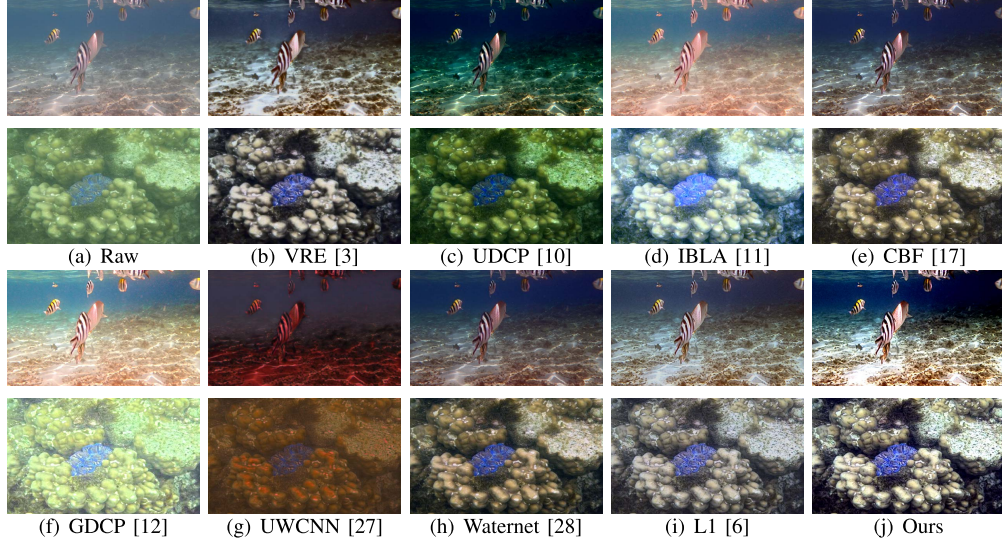


Fig. 9. Visual comparison of different methods on underwater images with other color degenerations.

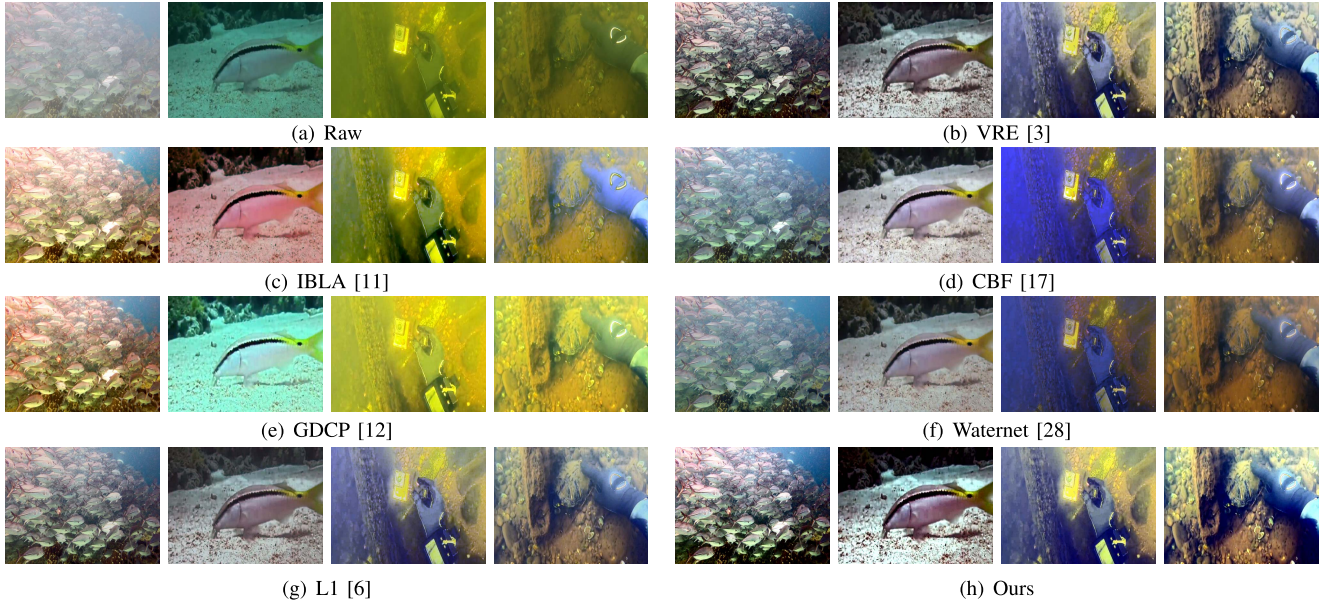


Fig. 10. Comparison of different methods on challenging underwater images from UIEBD [28].



Fig. 11. Underwater video enhanced by our method.

LOE are used to assess enhanced results. As reported, the proposed method substantially improves all metrics compared with VRE and L1, which uncovers that our hyper-Laplacian reflectance priors are able to eliminate both underwater structural ambiguity and underwater color distortions. For structural enhancement, our method yields higher numbers of restored visible edges than other methods, and our UISM values are ranked top in most cases. For contrast enhancement, the Con_l

of our method is ranked best for all cases, and our UIConM values are best in most cases. For color distortion removal, our LOE values are lower than those of most comparison methods.

Moreover, Fig. 12 reports three metrics PSNR, RMSE and LOE to quantify color correction accuracy of different methods. We first extract the color block part in these results, and then match the size and orientation of color block part to the ground-truth ColorChecker of the 24 X-Rite Chart

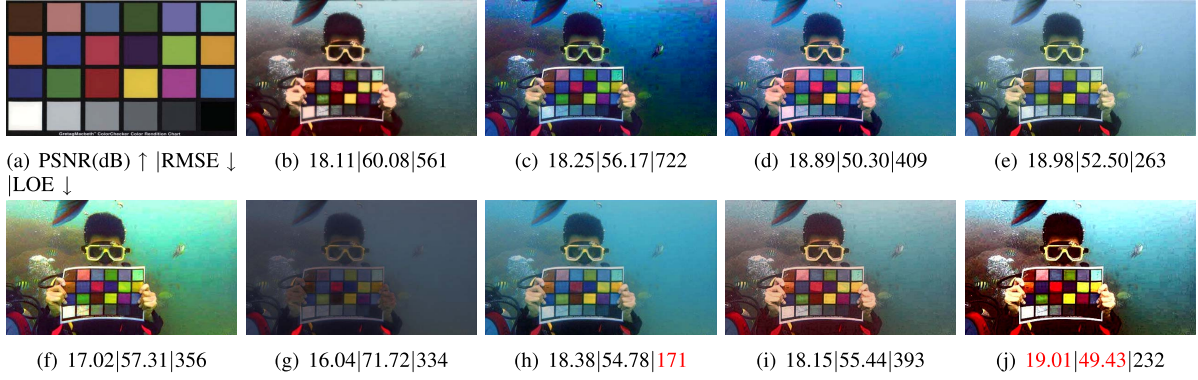


Fig. 12. Evaluation of color correction accuracy. (a) Ground truth, (b) VRE [3], (c) UDCP [10], (d) IBLA [11], (e) CBF [17], (f) GDCP [12], (g) UWCNN [27], (h) Waternet [28], (i) L1 [6], and (j) Ours.

TABLE II

METRICS (UISM ↑ | UICONM ↑ | Con_l ↑ | NVE ↑ | LOE ↓) OF DIFFERENT METHODS FOR ENHANCING UNDERWATER IMAGES OF DIFFERENT COLORS. THE BEST RESULT IS IN RED UNDER EACH CASE. ‘-’ INDICATES THE RESULT IS NOT AVAILABLE

Methods	Turtle	Fish	Tank	Coral
Raw	4.929 0.673 0.564 3463 -	7.295 0.773 0.839 1123 -	2.034 0.371 0.384 203 -	2.702 0.336 0.439 222 -
VRE [3]	5.315 0.807 0.854 86872 518	7.025 0.751 0.839 1111 122	3.481 0.672 0.831 3444 453	5.045 0.839 0.803 172875 343
UDCP [10]	4.355 0.603 0.768 40274 304	6.902 1.082 0.937 1706 242	2.481 0.559 0.692 10779 421	2.916 0.512 0.596 33590 303
IBLA [11]	4.677 0.614 0.749 37600 208	4.945 0.461 0.929 2984 278	2.677 0.454 0.541 702 342	3.362 0.385 0.608 6687 227
CBF [17]	5.689 0.816 0.892 85924 113	7.349 0.796 0.909 2444 51	3.334 0.655 0.858 4080 120	4.359 0.726 0.871 17013 159
GDCP [12]	7.221 1.224 0.929 10931 466	3.483 0.710 0.811 432 68	3.003 0.432 0.447 379 224	4.987 0.433 0.502 1240 384
UWCNN [27]	4.831 0.788 0.506 3050 204	7.234 0.736 0.643 584 64	2.291 0.487 0.404 644 333	2.992 0.602 0.443 308 221
Waternet [28]	5.341 0.816 0.709 33551 195	7.052 0.763 0.808 1323 35	2.843 0.614 0.576 1973 262	4.357 0.787 0.671 9651 174
L1 [6]	5.822 0.821 0.745 101961 350	7.308 0.743 0.678 1154 43	3.799 0.710 0.733 7127 312	5.342 0.833 0.745 388622 222
Ours	6.772 0.822 0.968 319944 216	7.395 1.682 0.947 6211 31	3.859 0.725 0.988 25239 234	5.395 0.841 0.898 593407 193

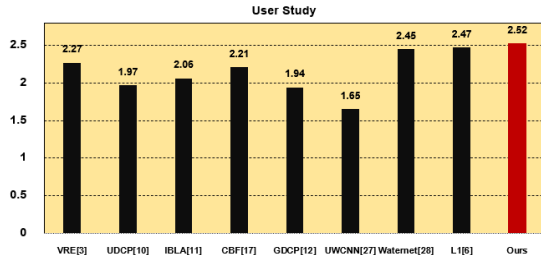


Fig. 13. User study for different methods on the 60 challenging underwater images from UIEBD [28].

image. The PSNR and RMSE are computed using the adjusted color block part and the ground-truth ColorChecker. We take the above similar operation to compute the LOE, but the difference is that the matching reference is the raw input image. As shown in Fig. 12, our method yields higher PSNR, lower RMSE, and lower LOE, which verifies the superiority of hyper-Laplacian reflectance priors in color and naturalness restoration accuracy.

In addition, we conduct a user study to assess visual results of different methods on the 60 challenging underwater images. We invite 100 volunteers to score the perceptual quality of the enhanced images by different methods. All participants are separately asked to score each image from 1 to 5 according to the visual quality, where 1 denotes the worst quality and

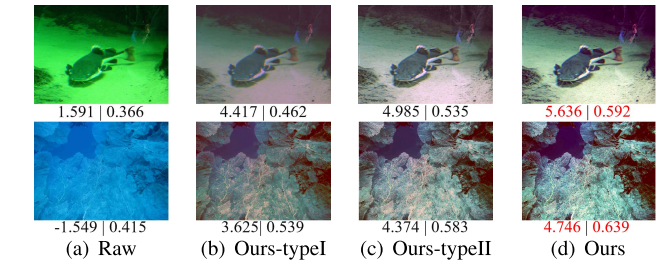


Fig. 14. Ablation study. UIQM|UCIQE are shown below and best results are red.

5 is the best quality. The visual quality relies on the results of color restoration and naturalness, structure and contrast improvement, artifacts and noise removal. Fig. 13 shows average scores of the results by each method on these challenging underwater images. As compared in Fig. 13, our method gains highest average score, which suggests that our method yields better results in a subjective study.

C. Ablation Study

To demonstrate the effect of each component in our model, we conduct an ablation study on two underwater images of different typical degradations, including the following experiments: 1) our model without retinex variational enhancement and illumination adjustment (Ours-typeI), 2) our model

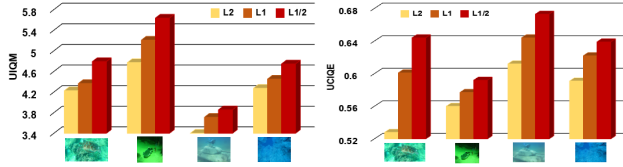


Fig. 15. Different norm comparison of reflectance penalty.

TABLE III
RUNTIME COMPARISON FOR DIFFERENT METHODS. THE BEST RESULT IS
IN RED UNDER EACH CASE

Methods	256×256	512×512	1024×1024
VRE [3]	0.056	0.217	1.120
UDCP [10]	5.029	17.776	92.481
IBLA [11]	8.330	34.025	144.286
CBF [17]	2.207	6.919	23.182
GDCP [12]	3.554	3.797	3.808
UWCNN [27]	0.0012	0.0025	0.011
Waternet [28]	0.022	0.098	0.38
L1 [6]	0.985	2.419	8.558
Ours	1.454	1.624	2.096

without illumination adjustment (Ours-typeII), 3) our full model (Ours). Fig. 14 displays enhanced results of Ours-typeI, Ours-typeII, and Ours, and the corresponding UIQM and UCIQE are reported below each image. As shown, Ours-I removes color casts and improves UIQM and UCIQE values. Ours-II boosts image structures and color restoration, meanwhile, UIQM and UCIQE values are further improved. Ours recovers more details and color naturalness, and is superior to Ours-II and Ours-I. Our full model yields best UIQM and UCIQE that exhibit the positive effect of each component in our model.

Furthermore, Fig. 15 shows different norm comparison of reflectance penalty under our model. Compared with both Gaussian and Laplacian reflectance priors, hyper-Laplacian reflectance priors yields higher UIQM and UCIQE. The $l_{1/2}$ norm better approximates empirical statistics of multi-order gradient of the reflectance, and is more accurate than the l_2 and l_1 norms for the reflectance penalty. This consequence further validates our motivation.

D. Runtime Comparison

We compare the runtime of different methods in Table III. Two deep learning-based methods UWCNN and Waternet are run on a Ubuntu 16.04 PC with an NVIDIA GeForce GTX 1080Ti GPU, and the average runtime of each method is executed one hundred times on images of different sizes. The rest traditional methods are run on a Windows 10 PC with Intel Core i7-10700K CPU at 3.79 GHz, 32G RAM and Matlab R2020a, and the average runtime of each method is executed one hundred times on images of different sizes. As shown in Table III, deep learning-based methods have obvious speed advantages thanks to the GPU acceleration. Based on fast element-wise operations and independent of additional underwater priors, our method achieves a competitive-to-better runtime when compared with other traditional approaches. The

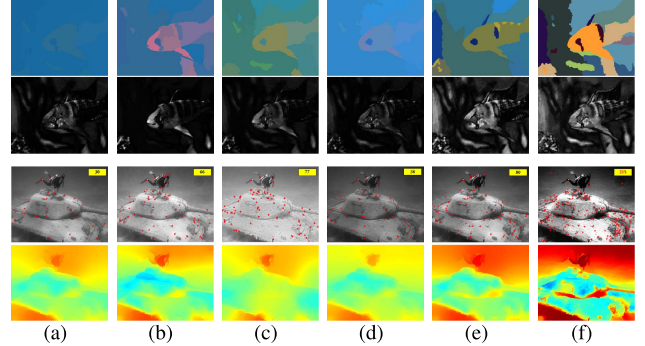


Fig. 16. Application examples of underwater image segmentation (top row), saliency detection (second row), keypoint detection (third row), and depth estimation (bottom row). (a) Raw. (b) IBLA [11]. (c) GDCP [12]. (d) UWCNN [27]. (e) Waternet [28]. (f) Ours.

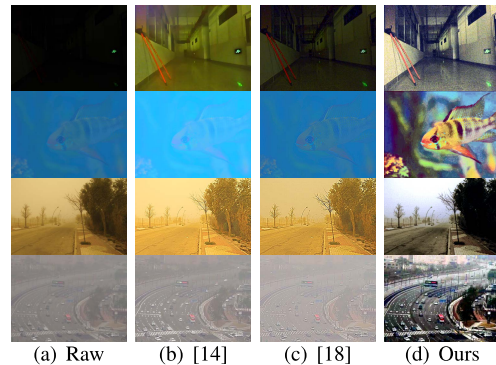


Fig. 17. Enhancement of different types of low-quality images.

fast processing speed and simple implementation pipeline of our method would benefit many practical applications.

E. Application Test

We show the utility of our method for several challenging applications without any parameter fine-tuning. First, we respectively adopt a superpixel-based clustering algorithm [45] and a graph-based manifold ranking method [47] to segment the enhanced results using different methods and detect corresponding saliency. In Fig. 16, the segmentation images of our method are more consistent and accurate than those of other methods, and our advantage is remarkable in the places of foreground objects and segmentation boundaries. Meanwhile, the saliency maps by our method contain more salient objects and better boundaries compared to those of other methods. These tests suggest that the proposed method is more effective for improving the performance of both underwater image segmentation and underwater saliency detection. Then, we respectively use the SIFT keypoint detection [46] and the transmission estimation [48] to detect underwater keypoints of the enhanced images by different methods and estimate the corresponding depth maps. In Fig. 16, our method substantially yields both more keypoint numbers and more accurate depth maps than other competitors. These results demonstrate that the proposed method recovers more crucial features that are beneficial to subsequent underwater object

detection and recognition. Last, the proposed method is compared with the two leading retinex models [14], [18] in enhancing low-light, underwater, sandstorm and hazy images. As shown in Fig. 17, better visibility and more details are enhanced by the proposed method, which suggests the better generalization of our method in enhancing different types of low-quality images.

VI. CONCLUSION

We have presented a hyper-laplacian reflectance priors for underwater image enhancement. In the proposed hyper-laplacian reflectance priors, 1) the $l_{1/2}$ -norm is more accurate to penalize multi-order gradients of the reflectance, which improves underwater image edges and details and recovers the authentic color naturalness; and 2) the l_2 norm is effective to enforce spatial smoothness and linear smoothness on the illumination. Extensive experiments show the superiority of our method in both qualitative and quantitative results.

REFERENCES

- [1] D. Akkaynak and T. Treibitz, "Sea-Thru: A method for removing water from underwater images," in *Proc. IEEE/CVF Conf. Comput. Vis. Pattern Recognit. (CVPR)*, Jun. 2019, pp. 1682–1691.
- [2] C. Ancuti, C. O. Ancuti, T. Haber, and P. Bekaert, "Enhancing underwater images and videos by fusion," in *Proc. IEEE Conf. Comput. Vis. Pattern Recognit.*, Jun. 2012, pp. 81–88.
- [3] X. Fu, P. Zhuang, Y. Huang, Y. Liao, X.-P. Zhang, and X. Ding, "A Retinex-based enhancing approach for single underwater image," in *Proc. IEEE Int. Conf. Image Process. (ICIP)*, Oct. 2014, pp. 4572–4576.
- [4] J. Xiong, Y. Dai, and P. Zhuang, "Underwater image enhancement by Gaussian curvature filter," in *Proc. IEEE 4th Int. Conf. Signal Image Process. (ICSIP)*, Jul. 2019, pp. 1026–1030.
- [5] Z. Zhao, Y. Dai, and P. Zhuang, "Underwater image enhancement with a total generalized variation illumination prior," in *IEEE Intl. Conf. Parallel Distrib. Process. Appl.*, Dec. 2019, pp. 1041–1048.
- [6] P. Zhuang, C. Li, and J. Wu, "Bayesian Retinex underwater image enhancement," *Eng. Appl. Artif. Intell.*, vol. 101, May 2021, Art. no. 104171.
- [7] M.-H. Cheng, T.-Z. Huang, X.-L. Zhao, T.-H. Ma, and J. Huang, "A variational model with hybrid hyper-Laplacian priors for Retinex," *Appl. Math. Model.*, vol. 66, pp. 305–321, Feb. 2019.
- [8] P. Drews, Jr., E. Do Nascimento, F. Moraes, S. Botelho, and M. Campos, "Transmission estimation in underwater single images," in *Proc. IEEE Int. Conf. Comput. Vis. Workshops*, Dec. 2013, pp. 825–830.
- [9] A. Galdran, D. Pardo, A. Picón, and A. Alvarez-Gila, "Automatic red-channel underwater image restoration," *J. Vis. Commun. Image Represent.*, vol. 26, pp. 132–145, Jan. 2015.
- [10] P. Drews, Jr., E. R. Nascimento, S. S. C. Botelho, and M. F. M. Campos, "Underwater depth estimation and image restoration based on single images," *IEEE Comput. Graph. Appl.*, vol. 36, no. 2, pp. 24–35, Mar./Apr. 2016.
- [11] Y.-T. Peng and P. C. Cosman, "Underwater image restoration based on image blurriness and light absorption," *IEEE Trans. Image Process.*, vol. 26, no. 4, pp. 1579–1594, Apr. 2017.
- [12] Y.-T. Peng, K. Cao, and P. C. Cosman, "Generalization of the dark channel prior for single image restoration," *IEEE Trans. Image Process.*, vol. 27, no. 6, pp. 2856–2868, Jun. 2018.
- [13] J. Y. Chiang and Y.-C. Chen, "Underwater image enhancement by wavelength compensation and dehazing," *IEEE Trans. Image Process.*, vol. 21, no. 4, pp. 1756–1769, Apr. 2012.
- [14] M. Li, J. Liu, W. Yang, X. Sun, and Z. Guo, "Structure-revealing low-light image enhancement via robust Retinex model," *IEEE Trans. Image Process.*, vol. 27, no. 6, pp. 2828–2841, Jun. 2018.
- [15] M. S. Hitam, W. N. J. H. W. Yussof, E. A. Awalludin, and Z. Bachok, "Mixture contrast limited adaptive histogram equalization for underwater image enhancement," in *Proc. Int. Conf. Comput. Appl. Technol. (ICCAT)*, Jan. 2013, pp. 1–5.
- [16] S. Zhang, T. Wang, J. Dong, and H. Yu, "Underwater image enhancement via extended multi-scale Retinex," *Neurocomputing*, vol. 245, Jul. 2017, pp. 1–9.
- [17] C. O. Ancuti, C. De Vleeschouwer, and P. Bekaert, "Color balance and fusion for underwater image enhancement," *IEEE Trans. Image Process.*, vol. 27, no. 1, pp. 379–393, Jan. 2018.
- [18] X. Ren, W. Yang, W.-H. Cheng, and J. Liu, "LR3M: Robust low-light enhancement via low-rank regularized Retinex model," *IEEE Trans. Image Process.*, vol. 29, pp. 5862–5876, 2020.
- [19] B. Cai, X. Xu, K. Jia, C. Qing, and D. Tao, "DehazeNet: An end-to-end system for single image haze removal," *IEEE Trans. Image Process.*, vol. 25, no. 11, pp. 5187–5198, Nov. 2016.
- [20] K. Zhang, W. Zuo, Y. Chen, D. Meng, and L. Zhang, "Beyond a Gaussian denoiser: Residual learning of deep CNN for image denoising," *IEEE Trans. Image Process.*, vol. 26, no. 7, pp. 3142–3155, Jul. 2017.
- [21] C. Dong, C. C. Loy, K. He, and X. Tang, "Image super-resolution using deep convolutional networks," *IEEE Trans. Pattern Anal. Mach. Intell.*, vol. 38, no. 2, pp. 295–307, Feb. 2016.
- [22] J. Li, K. A. Skinner, R. M. Eustice, and M. Johnson-Roberson, "WaterGAN: Unsupervised generative network to enable real-time color correction of monocular underwater images," *IEEE Robot. Autom. Lett.*, vol. 3, no. 1, pp. 387–394, Jan. 2018.
- [23] I. Goodfellow *et al.*, "Generative adversarial nets," in *Proc. Adv. Neural Inf. Process. Syst.*, 2014, pp. 2672–2680.
- [24] J.-Y. Zhu, T. Park, P. Isola, and A. A. Efros, "Unpaired image-to-image translation using cycle-consistent adversarial networks," in *Proc. IEEE Int. Conf. Comput. Vis. (ICCV)*, Oct. 2017, pp. 81–88.
- [25] C. Li, J. Guo, and C. Guo, "Emerging from water: Underwater image color correction based on weakly supervised color transfer," *IEEE Signal Process. Lett.*, vol. 25, no. 3, pp. 323–327, Mar. 2018.
- [26] C. Fabbri, M. J. Islam, and J. Sattar, "Enhancing underwater imagery using generative adversarial networks," in *Proc. IEEE Int. Conf. Robot. Autom. (ICRA)*, May 2018, pp. 7159–7165.
- [27] C. Li, S. Anwar, and F. Porikli, "Underwater scene prior inspired deep underwater image and video enhancement," *Pattern Recognit.*, vol. 98, pp. 1204–1211, Feb. 2020.
- [28] C. Li *et al.*, "An underwater image enhancement benchmark dataset and beyond," *IEEE Trans. Image Process.*, vol. 29, pp. 4376–4389, 2019.
- [29] J. Sattar and G. Dudek, "On the performance of color tracking algorithms for underwater robots under varying lighting and visibility," in *Proc. IEEE Int. Conf. Robot. Autom. (ICRA)*, 2006, pp. 3550–3555.
- [30] E. H. Land and J. J. McCann, "Lightness and Retinex theory," *J. Opt. Soc. Amer.*, vol. 61, no. 1, pp. 1–11, 1971.
- [31] H. Yue, J. Yang, X. Sun, F. Wu, and C. Hou, "Contrast enhancement based on intrinsic image decomposition," *IEEE Trans. Image Process.*, vol. 26, no. 8, pp. 3981–3994, Aug. 2017.
- [32] X. Fu, Y. Liao, D. Zeng, Y. Huang, X. Zhang, and X. Ding, "A probabilistic method for image enhancement with simultaneous illumination and reflectance estimation," *IEEE Trans. Image Process.*, vol. 24, no. 12, pp. 4965–4977, Dec. 2015.
- [33] S. Boyd, N. Parikh, E. Chu, B. Peleato, and J. Eckstein, "Distributed optimization and statistical learning via the alternating direction method of multipliers," *Found. Trends Mach. Learn.*, vol. 3, no. 1, pp. 1–122, Nov. 2011.
- [34] J. Zeng, S. Lin, Y. Wang, and Z. Xu, " $L_{1/2}$ regularization: Convergence of iterative half thresholding algorithm," *IEEE Trans. Signal Process.*, vol. 62, no. 9, pp. 2317–2329, May 2014.
- [35] Z. Xu, X. Chang, F. Xu, and H. Zhang, " $L_{1/2}$ regularization: A thresholding representation theory and a fast solver," *IEEE Trans. Neural Netw. Learn. Syst.*, vol. 23, no. 7, pp. 1013–1027, May 2012.
- [36] M. K. Ng and W. Wang, "A total variation model for Retinex," *SIAM J. Imag. Sci.*, vol. 4, no. 1, pp. 345–365, Jan. 2011.
- [37] Z.-U. Rahman, D. J. Jobson, and G. A. Woodell, "Retinex processing for automatic image enhancement," *J. Electron. Imag.*, vol. 13, no. 1, pp. 100–110, 2004.
- [38] D. J. Jobson, Z.-U. Rahman, and G. A. Woodell, "Properties and performance of a center/surround Retinex," *IEEE Trans. Image Process.*, vol. 6, no. 3, pp. 451–462, Mar. 1997.
- [39] C.-Y. Li, J.-C. Guo, R.-M. Cong, Y.-W. Pang, and B. Wang, "Underwater image enhancement by dehazing with minimum information loss and histogram distribution prior," *IEEE Trans. Image Process.*, vol. 25, no. 12, pp. 5664–5677, Dec. 2016.
- [40] C. Li, J. Guo, C. Guo, R. Cong, and J. Gong, "A hybrid method for underwater image correction," *Pattern Recognit. Lett.*, vol. 94, pp. 62–67, Jul. 2017.
- [41] K. Panetta, C. Gao, and S. Agaian, "Human-visual-system-inspired underwater image quality measures," *IEEE J. Ocean Eng.*, vol. 41, no. 3, pp. 1–11, Jul. 2015.

- [42] M. Yang and A. Sowmya, "An underwater color image quality evaluation metric," *IEEE Trans. Image Process.*, vol. 24, no. 12, pp. 6062–6071, Dec. 2015.
- [43] S. Wang, K. Ma, H. Yeganeh, Z. Wang, and W. Lin, "A patch-structure representation method for quality assessment of contrast changed images," *IEEE Signal Process. Lett.*, vol. 22, no. 12, pp. 2387–2390, Dec. 2015.
- [44] N. Hautière, J.-P. Tarel, D. Aubert, and É. Dumont, "Blind contrast enhancement assessment by gradient ratioing at visible edges," *Image Anal. Stereol. J.*, vol. 27, no. 2, pp. 87–95, Jun. 2011.
- [45] T. Lei, X. Jia, Y. Zhang, S. Liu, H. Meng, and A. K. Nandi, "Superpixel-based fast fuzzy C-Means clustering for color image segmentation," *IEEE Trans. Fuzzy Syst.*, vol. 27, no. 9, pp. 1753–1766, Sep. 2019.
- [46] D. G. Lowe, "Distinctive image features from scale-invariant keypoints," *Int. J. Comput. Vis.*, vol. 60, no. 2, pp. 91–110, 2004.
- [47] C. Yang, L. Zhang, H. Lu, X. Ruan, and M.-H. Yang, "Saliency detection via graph-based manifold ranking," in *Proc. IEEE Conf. Comput. Vis. Pattern Recognit.*, Jun. 2013, pp. 3166–3173.
- [48] D. Berman, T. Treibitz, and S. Avidan, "Non-local image dehazing," in *Proc. IEEE Conf. Comput. Vis. Pattern Recognit. (CVPR)*, Jun. 2016, pp. 1674–1682.
- [49] Z. Rahman, M. Aamir, Y.-F. Pu, F. Ullah, and Q. Dai, "A smart system for low-light image enhancement with color constancy and detail manipulation in complex light environments," *Symmetry*, vol. 10, no. 12, p. 718, Dec. 2018.



Peixian Zhuang received the Ph.D. degree from the School of Informatics, Xiamen University, Xiamen, China, in 2016. From 2017 to 2020, he was a Lecturer and a Master Supervisor with the School of Electronics and Information Engineering, Nanjing University of Information Science and Technology, Nanjing, China. He is currently a Postdoctoral Fellow with the Department of Automation, Tsinghua University, Beijing, China. He has published over 30 peer-reviewed papers in Image Processing and Computer Vision. His research interests include sparse representation, Bayesian modeling, deep learning, and calcium signal processing. He was a recipient of the Outstanding Doctoral Dissertations of Fujian province in 2017. He has served as a Reviewer for the IEEE TRANSACTIONS ON IMAGE PROCESSING, IEEE TRANSACTIONS ON CIRCUITS AND SYSTEMS FOR VIDEO TECHNOLOGY, IEEE TRANSACTIONS ON GEOSCIENCE AND REMOTE SENSING, IEEE TRANSACTIONS ON COMPUTATIONAL IMAGING, and IEEE TRANSACTIONS ON CONSUMER ELECTRONICS; the Guest Editor for the *Journal of Electronics and Information Technology* in 2021; and the Session Chair for the IEEE International Conference on Signal and Image Processing in 2019.



Jiamin Wu received the B.S. and Ph.D. degrees in automation from Tsinghua University, Beijing, China, in 2014 and 2019, respectively. He is currently an Assistant Professor with the Department of Automation, Tsinghua University. He has published over 20 peer-reviewed articles in *Cell*, *Nature Photonics*, *Nature Methods*, *Nature Machine Intelligence*, and *Physical Review Letters*. His current research interests focus on computational microscopy and optical computing, with a particular emphasis on developing computation-based optical setups for observing large-scale biological dynamics *in vivo*. He has served as the Associate Editor for the IEEE TRANSACTIONS ON CIRCUITS AND SYSTEMS FOR VIDEO TECHNOLOGY, and the Reviewers for *Light: Science and Applications*, *Optica*, and *Optics Express*.



Fatih Porikli received the Ph.D. degree from New York University, New York, NY, USA, in 2002. He was a Distinguished Research Scientist with the Mitsubishi Electric Research Laboratories, Cambridge, MA, USA. He was a full-tenured Professor with the Research School of Engineering, The Australian National University, Canberra, ACT, Australia, and a Chief Scientist with the Global Media Technologies Laboratory, Huawei, Santa Clara, CA, USA. He is currently the Global Lead of Perception with Qualcomm, San Diego, CA. He has authored over 300 publications, co-edited two books, and invented 66 patents. His research interests include computer vision, pattern recognition, manifold learning, image enhancement, robust and sparse optimization, and online learning with commercial applications in video surveillance, car navigation, robotics, satellite, and medical systems. He was a recipient of the Research and Development 100 Scientist of the Year Award in 2006. He has also received five best paper awards from premier IEEE conferences and five other professional prizes. He is serving as an associate editor for several journals for the past 12 years. He has served on the organizing committees of several flagship conferences, including International Conference on Computer Vision (ICCV), European Conference on Computer Vision (ECCV), and Computer Vision and Pattern Recognition (CVPR).



Chongyi Li (Member, IEEE) received the Ph.D. degree from the School of Electrical and Information Engineering, Tianjin University, Tianjin, China, in June 2018. From 2016 to 2017, he was a joint-training Ph.D. Student with The Australian National University, Australia. He was a Research Fellow with the City University of Hong Kong and Nanyang Technological University, Singapore, from 2018 to 2021. He is currently a Research Assistance Professor with the School of Computer Science and Engineering, Nanyang Technological University. His current research focuses on image processing, computer vision, and deep learning, particularly in the domains of image restoration and enhancement.